THE JOURNAL OF PHYSICAL CHEMISTRY C
A JOURNAL OF THE AMERICAN CHEMICAL SOCIETY

pubs.acs.org/JPCC

Article

Deuterium NMR Studies of the Solid–Liquid Phase Transition of Octanol-d_{17} Confined in SBA-15

Sonja C. Döller, Martin Brodrecht, Nadia B. Haro Mares, Hergen Breitzke, Torsten Gutmann, Markus Hoffmann, and Gerd Buntkowsky*

Cite This: J. Phys. Chem. C 2021, 125, 25155–25164

Read Online

ACCESS | Metrics & More | Article Recommendations | Supporting Information

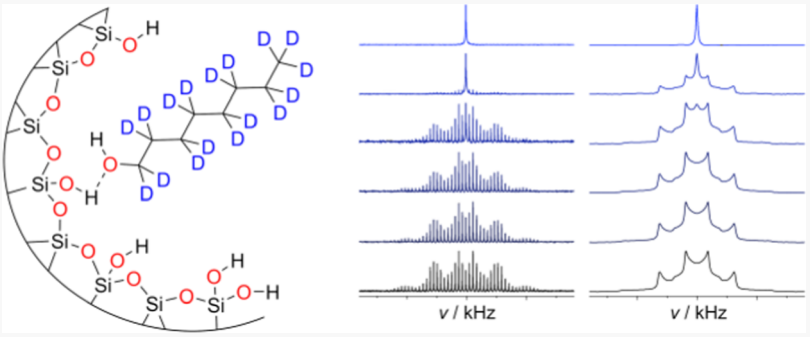

ABSTRACT: The interactions of molecules such as surfactants with solid interfaces are not sufficiently understood since their study is challenging with standard spectroscopic methods. In this work, octanol-d_{17} as a model system confined in the mesopores of SBA-15 is studied by variable temperature deuterium solid-state NMR, and the findings are compared to those of bulk octanol-d_{17}. The magic angle spinning (MAS) as well as the static, nonspinning case, are investigated, showing that the described observations are independent of the applied NMR method. The ^{2}H NMR spectra of both the bulk and the confined octanol-d_{17} show a large and a small quadrupolar Pake pattern below the melting point, suggesting a rigid conformation of the observed molecules with a 3-fold jump motion of the terminal CD_3-group. Apart from the melting of the solid, no other phase transition is observed for either sample. The confined octanol-d_{17} forms a pore solid, exhibiting a melting point 38 K lower than bulk octanol-d_{17}. The interactions of the molecule with the mesoporous SBA-15 bring about a distribution of activation energies for the melting process, resulting in a gradual melting process.

INTRODUCTION

Systems consisting of solid–liquid interfaces play a key role in many processes relevant to scientific and industrial applications. Heterogeneously catalyzed reactions,[1] liquid chromatography,[2] membrane-based separation processes,[3] drug delivery systems,[4] and waste-treatment systems,[5] among others, all rely on the interactions of a liquid phase and a solid adsorbent. Especially silica-based solid phases have been of interest due to their easy synthesis, their ordered structures, large surface areas, and the facile functionalization of their surfaces, allowing an adjustment of the material to the specific task.[6] These properties make silica-based systems ideal as model systems to investigate surface interactions and dynamics at a molecular level. Mesoporous systems, such as the class of Santa Barbara Amorphous[7] (SBA) and the family of M41S phases,[8] have been used as host materials to a plethora of guest molecules.[9−17]

One of the most interesting classes of guest molecules is surfactants. Due to their amphiphilic nature, they form aggregates like micelles and mono- as well as bilayer lamellae on their own[10,18−21] and in aqueous solution.[22−26] Typically, if the surfactants interact with a solid, different aggregates are formed compared to the behavior in their bulk solution without the influence of a surface.[27,28] However, despite the relevance and countless applications of these systems, the corresponding interactions are not fully understood and notoriously hard to probe at a molecular level, impeding the optimization of the utilized methods of analysis.[29] Recently, there have been advances in the fields of infrared,[30] Raman,[31] UV–vis,[32] and fluorescence emission spectroscopy,[33] as well as X-ray[34] and neutron-scattering[35]-based techniques to investigate adsorption on surfaces. Nonetheless, these techniques do not necessarily enable the observation of molecules confined in pores and their dynamics as closely as needed to gather a

Received: July 1, 2021
Revised: October 20, 2021
Published: November 4, 2021

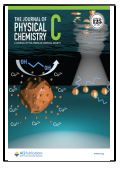

https://doi.org/10.1021/acs.jpcc.1c05873
J. Phys. Chem. C 2021, 125, 25155–25164

deeper understanding of the interactions taking place. Consequently, ^{2}H solid-state NMR (ssNMR) has become an established method to study these systems. Due to the deuterium quadrupolar moment, the line shape of ^{2}H ssNMR spectra is highly sensitive to dynamic processes. Therefore, ^{2}H ssNMR spectra directly probe the movement of the compound of interest or dynamics of the structural moieties bearing deuterium at a molecular level, revealing information about rotational and translational movements, the binding situation, or sorption kinetics while being specific to the probed compound.[36]

In this work, octanol-d_{17} is used as a characteristic model compound for the class of linear, nonionic, and aliphatic surfactants. It is structurally similar to lipids found in biological membranes and therefore used as a membrane mimetic.[37,38] The water-octanol partition coefficient is employed as a measure to describe the partitioning of solutes between aqueous (hydrophilic) and organic (lipophilic) phases[13,15,16] and to predict the pharmacokinetic properties of drug molecules.[19−21] Octanol has been shown to interact with the surface of SBA-15 via its hydroxyl group,[10] but little is known about the dynamics of the aliphatic moiety of the molecule, making it an interesting compound for ^{2}H ssNMR studies in confinement at low temperatures and around its melting point. The spectra of bulk octanol-d_{17} are employed as reference to distinguish the effects of the confinement. The data obtained by differential scanning calorimetry (DSC) measurements is used to aid in understanding the observed phase transition. Modeling in accordance with Kissinger[39] and Rössler et al.[40] serves to elucidate the influence of the confinement on the temperature as well as the activation energy profile of the melting process. A detailed discussion on confinement effects on small molecules is beyond the scope of this paper and can be found in a recent review[41] and references therein.

The rest of the paper is organized as follows: first, the Experimental Methods section gives an overview of the synthesis and characterization of the utilized SBA-15 porous material, the sample preparation, the low-temperature DSC methods, as well as the applied ^{2}H NMR methods for obtaining static and magic angle spinning (MAS) spectra. Subsequently, the findings of this work are presented and discussed, starting with the DSC measurements and followed by the NMR investigation. In particular, the influence of confinement on the dynamics of octanol-d_{17} is discussed. A summary of the key findings and their applicability is provided in the Conclusions section.

EXPERIMENTAL METHODS

General. Information on the utilized chemicals can be found in Table S1 in the Supporting Information. All chemicals were used as received. The octanol-d_{17} as well as the mesoporous SBA-15 were stored in a glovebox under argon to prevent wetting of the sample with atmospheric water.

Synthesis of Mesoporous SBA-15. Mesoporous SBA-15 was synthesized via a literature-based protocol.[42,43] Accordingly, 21.3 g (0.017 equiv) of Pluronic123 was dissolved in 574 mL (165 equiv) of deionized water overnight. To the solution, 108.0 mL (6.0 equiv) of 37 wt % HCl was added to yield a HCl concentration of 1.9 mol L^{-1}. The solution was heated to 40 °C and allowed to equilibrate overnight. After that, 47.9 g (1 equiv) of tetraethyl orthosilicate was added slowly while stirring. Stirring was continued for 1 h, which resulted in a white precipitate. The suspension was stirred at 40 °C for 24 h and was then transferred into a Teflon (PTFE) bottle. The bottle was stored under static conditions at 90 °C for 48 h. The white precipitate was washed with deionized water twice and with ethanol once by centrifugation. The leftover template was removed by calcination at 650 °C yielding 11.70 g of SBA-15 mesoporous silica.

Porosity, Pore Volume, and Specific Surface Area of the Mesoporous SBA-15. In preparation of characterizing the synthesized SBA-15 porous material, the wet samples were transferred into a glass burette and predried at mild vacuum (∼10 mbar) overnight. After predrying, the samples were dried using a turbomolecular pump (10^{-6} mbar) overnight. During all drying steps, the samples were heated to 80 °C. The dried samples were directly transferred to a Thermo Fisher Scientific Surfer Brunauer−Emmett−Teller (BET) analyzer, which obtains the porosity, pore volume, and specific surface area of the material by controlled nitrogen adsorption at 77 K. The specific surface area was obtained by the Brunauer−Emmett−Teller[44] (BET) method, analyzing the curve in the p/p^0 range between 0.1 and 0.35. The pore volume was obtained by the Klyachko-Gurvich[45] method, using the p/p^0 value at 0.95. Blank measurements were performed using helium gas. Pore size distributions were obtained by applying the Barrett−Joyner−Halenda[46] (BJH) method, analyzing the adsorption−desorption isotherms in the p/p^0 range between 0.3 and 0.95. Pore sizes were obtained by nonlocal density functional theory (NLDFT) based on the model for the adsorption of nitrogen on silica surfaces with cylindrical pore geometries of Advanced Data Processing (ADP) software (V 6.2.4). The samples used for BET measurements were discarded and not used for ssNMR or DSC measurements. The obtained isotherms are visualized in Figure S1 in the Supporting Information.

Sample Preparation for ssNMR and DSC Measurements. In preparation for the impregnation with octanol-d_{17}, the SBA-15 material (d = 6.4 nm; S = 555 m^2 g^{-1}; V = 0.79 cm^3 g^{-1}) was placed under high vacuum at room temperature for 24 h. The dried silica was then transferred to the glovebox as quickly as possible to avoid the material absorbing water from the atmosphere. Octanol-d_{17} was added to the material to fill approximately 80% of the pore volume, and the material was left in the glovebox overnight to allow the octanol-d_{17} to be absorbed by the mesoporous silica. Of this material, approximately 2 and 6.5 mg were used for the DSC and NMR measurements, respectively. The DSC cubicles as well as the MAS rotors were filled in the glovebox. Examples of the spectra measured before the sample was allotted enough time for the octanol-d_{17} to be absorbed can be found in Figure S2 in the Supporting Information.

DSC Measurements. The DSC measurements were performed in a dynamic mode on the DSC 214 Polyma apparatus by Netzsch using evaporated liquid nitrogen as the cooling agent with an empty crucible serving as the reference. Heating rates of 5, 10, 20, and 40 K min^{-1} were used. The temperature range was set between 100 and 300 K for all compounds. For the analysis according to Kissinger,[39] the peak temperatures of the DSC signals are determined.

Variable-Temperature ^{2}H Solid-State NMR Spectroscopy. *General.* All measurements were carried out on a Bruker Avance III 400 DNP NMR spectrometer operating at 9.4 T (400.13 MHz for ^{1}H, 61.42 MHz for ^{2}H) equipped with a 3.2 mm low-temperature H/X/Y triple resonance probe, which was used in H/Y double mode to obtain a higher Q-factor for ^{2}H on the Y-channel. The temperature was controlled by a

https://doi.org/10.1021/acs.jpcc.1c05873
J. Phys. Chem. C 2021, 125, 25155−25164

Eurotherm 2416 temperature controller with a Pt100 sensor. Typically, 3.2 mm sapphire rotors with Teflon inserts and ZrO_2 drive caps were used. The spectra were measured in the range of 120−260 K. After each temperature step, the sample was allowed 15 min to thermally equilibrate.

Temperature Calibration. For MAS measurements, the temperature of the sample was calibrated according to Bielecki and Burum.[47] For the static measurements, the temperature within the probe head was determined by taking the reading of the auxiliary sensor installed directly in the stator of the probe head. At the observed melting point of octanol-d_{17}, both methods yield a temperature reading that falls within 1.5 K. The temperature uncertainty was therefore taken as 1.5 K.

^{2}H Magic Angle Spinning Measurements. MAS experiments were acquired as onepulse experiments with a pulse length of 2 μs, approximately corresponding to a 30° pulse. 64 scans were acquired with a recycle delay of 1 s. The spectra were analyzed with the program dmfit2015[48] using the integrated option Quad 1st model. To model the shape of the spectra, two Pake patterns and one Lorentzian signal were used throughout the analysis.

^{2}H Static Measurements. The static experiments were performed in resonance with a solid-echo pulse sequence using an echo delay of 40 μs and a pulse length of 2.6 μs, approximately corresponding to a 90°-pulse. 1024 scans were acquired using a recycle delay of 15 s. The obtained data was phase-corrected by maximizing the echo amplitude and symmetrized by deleting the imaginary part of the signal before the Fourier transformation. The simulated spectra in this work were calculated and fitted onto the experimental data with a Matlab script written in house. An example of an original, nonsymmetrized spectrum, including a corresponding fit, can be found in Figure S3 in the Supporting Information.

RESULTS AND DISCUSSION

DSC Measurements. Figure 1 shows the obtained DSC curves for octanol-d_{17} confined in mesoporous SBA-15 for the smallest and largest heating rate. Both curves show characteristic signals at ∼220 K and at ∼258 K, which are assigned to the confined octanol-d_{17} and nonconfined, superfluous bulk octanol-d_{17}, respectively. This result containing the bulk as well as the confined signal was not used for the following analysis but served as an exemplary comparison for the signal line shape only.

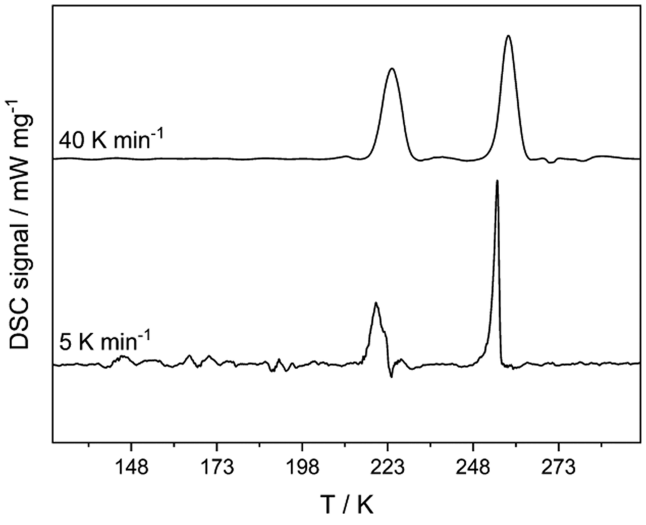

Figure 1. DSC curves for octanol-d_{17} in SBA-15 at 5 and 40 K min^{-1}. Heating rates are indicated in the figure. All curves are normalized to an equal height.

The DSC measurements yield the peak temperature of the sample for the different heating rates. According to Kissinger,[39] these peak temperatures can be used to calculate the activation energy E_A of the observed phase transition using the heating rate ν, the gas constant R, and the observed peak temperature T_p of the sample (eq 1). Since this model is not applicable to crystallization processes occurring under cooling conditions,[49] only the melting behavior of the samples under heating conditions is investigated.

$$\frac{\mathrm{d}\ln\left(\frac{\nu}{T_p^2}\right)}{\mathrm{d}\frac{1}{T_p}} = -\frac{E_A}{R} \tag{1}$$

Figure 2 displays the plots used to determine the activation energy of the phase transitions. The obtained data, including the determined activation energies, are shown in Table 1.

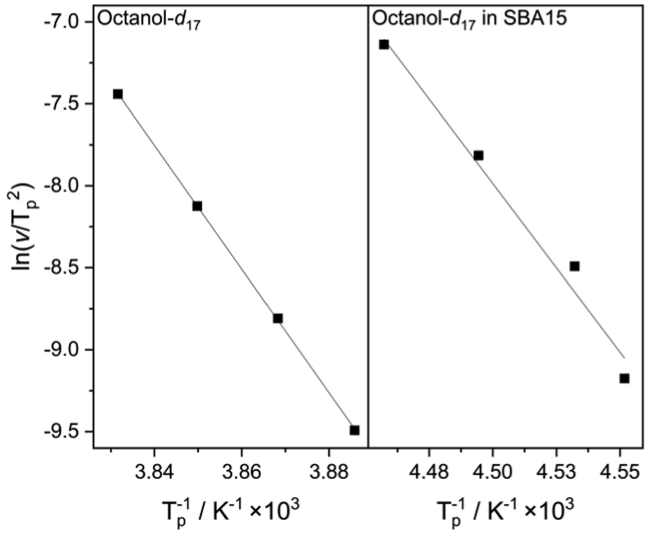

Figure 2. Kissinger plots for bulk octanol-d_{17} and for octanol-d_{17} in SBA-15.[39]

The octanol-d_{17} in SBA-15 melts at a temperature approximately 38 K lower than for bulk octanol-d_{17}, which can be interpreted as a result of confinement.[50] As expected from the observed lower melting point, the activation energy for the solid−liquid phase transition is smaller when octanol-d_{17} is confined. The relatively large error determined for the confined case stems from the observed broad scattering of peak temperatures. No other phase transition can be observed in the DSC measurements for either sample, which is in accordance with the literature.[51] The broader line shape of the melting DSC signature in Figure 1 for the confined octanol-d_{17} compared to the melting DSC signature of the crystalline bulk octanol-d_{17} indicates the presence of a variety of interactions of the guest molecule with the mesoporous SBA-15 surface, leading to different species with different melting points.[52] Considering the pore size of 6.5 nm, a full crystallization of the material in the pores is unlikely. Due to the interactions of the hydroxyl group of octanol-d_{17} with the pore walls, some order is probably established in the octanol-

https://doi.org/10.1021/acs.jpcc.1c05873
J. Phys. Chem. C 2021, 125, 25155−25164

Table 1. T_p and E_A of the Observed Phase Transition for Bulk Octanol-d_{17} and Octanol-d_{17} in SBA-15 for Different Heating Rates[a]

	T_p in K at				
material	5 K min^{-1}	10 K min^{-1}	20 K min^{-1}	40 K min^{-1}	E_A/kJ mol^{-1}
octanol-d_{17}	257.3	258.5	259.6	261.0	313.6 ± 2.10
octanol-d_{17} in SBA-15	219.7	220.6	222.3	224.4	172 ± 17

[a]Errors for E_A were determined based on the slope uncertainty.

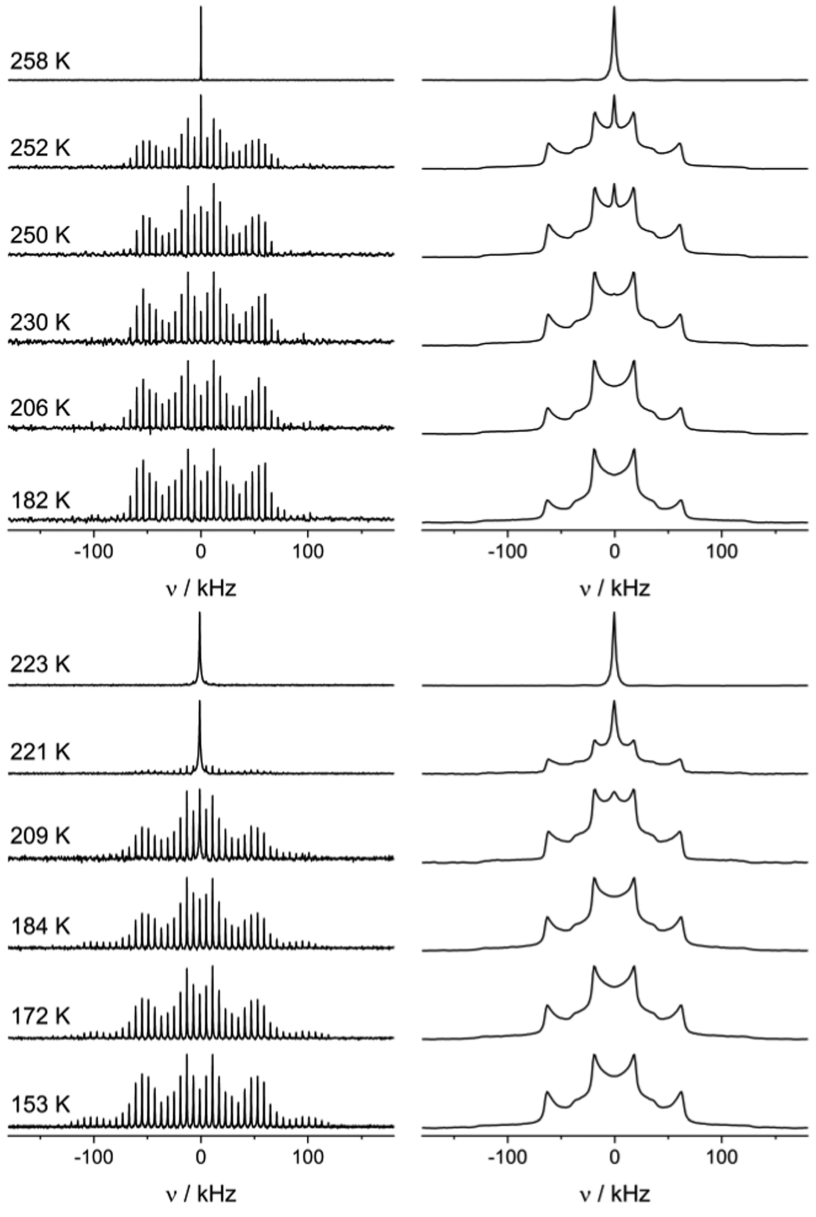

Figure 3. Select ^{2}H MAS NMR spectra (left side) and solid-echo ^{2}H spectra (right side) of bulk octanol-d_{17} (top row) and octanol-d_{17} confined in mesoporous SBA-15 (bottom row). Temperatures are indicated in the figure. All spectra are normalized to an equal height.

d_{17} layer close to the mesoporous material. However, toward the pore center, this order is unlikely to persist, possibly resulting in a strongly disordered, partially amorphous, or glasslike portion of the molecules.[10,52,53]

^{2}H NMR Spectra. Figure 3 shows a selection of the recorded ^{2}H NMR spectra to provide an overview of the effect of temperature on the spectral shapes. In this work, both MAS and static spectra are recorded so that as much information as possible are gathered on the molecular dynamics. Both experiments are echo experiments; however, the echo does not appear on the same time scale in both cases, possibly leading to different parts of the molecular dynamics being observable with different experiments. The MAS experiments have the big advantage that they are much faster compared to the solid-echo experiments (typically about 2 min versus 4 h of measuring time) per spectrum in our systems; the solid-echo experiments are more sensitive toward the detection of faster relaxing species.

https://doi.org/10.1021/acs.jpcc.1c05873
J. Phys. Chem. C 2021, 125, 25155−25164

The line shape of the experimental spectra results from a superposition of different spectral components. For the ^{2}H MAS NMR spectra, a large and a small Pake pattern are visible, with a Lorentzian signal emerging close to the melting point of the respective compound. The static spectra also display the Pake patterns as well as the Lorentzian signal close to the melting point. However, upon fitting these spectra, an additional component can be observed below the temperatures of 195 K for bulk octanol-d_{17} and 170 K for octanol-d_{17} in SBA-15 (shown exemplarily in Figure 4). This signal shows

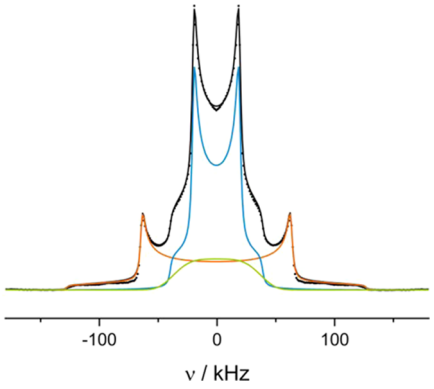

Figure 4. Solid-echo ^{2}H NMR spectrum of bulk octanol-d_{17} at 150 K with the overall fit (black solid line) and the fits of the different components (blue: narrow Pake pattern, orange: broad Pake pattern, green: broad non-Pake signal).

neither a Pake pattern nor a Lorentzian shape. It probably arises due to the dynamics of the corresponding deuterons falling within the NMR time scale at these temperatures, resulting in an intermediate exchange regime and therefore distortion of the signal and intensity loss due to the echo not being refocused by the second pulse.[54,55] The time scale of the echo observation is different in the MAS spectra than in the static spectra, potentially explaining why the signal cannot be observed in the MAS spectra due to motional broadening. This signal possibly corresponds to a less ordered portion of octanol-d_{17}.[10]

The hydroxyl group of the octanol-d_{17} does not produce a signal in the ^{2}H NMR since it is not deuterated. In this work, we refrained from using octanol-d_{18} since we expect the hydroxyl group to be susceptible to exchange processes, resulting in a partial loss of deuterium at this position. This would result in an uncertainty of the extracted numerical values for the determined intensities. Having the hydroxyl group deuterated would also lead to a further complication of the spectral shapes, making it more difficult to describe the dynamics of the aliphatic moiety of the molecules.

Generally, the melting points observed in the NMR experiments agree with those determined by the DSC measurements.

Figure 5 shows the quadrupolar coupling constant, C_Q, which was extracted via numerical modeling from all recorded spectra as a function of temperature T. At 258 and 223 K, respectively, only the Lorentzian signal (i.e., $C_Q = 0$) can be observed, indicating a full melting of the sample.

The large Pake pattern shows $C_Q \approx 170$ kHz just until the melting point, a value typical for an immobile deuteron of a −CD bond.[56] The quadrupolar coupling constant of the smaller Pake pattern is obtained as $C_Q \approx 55$ kHz, suggesting

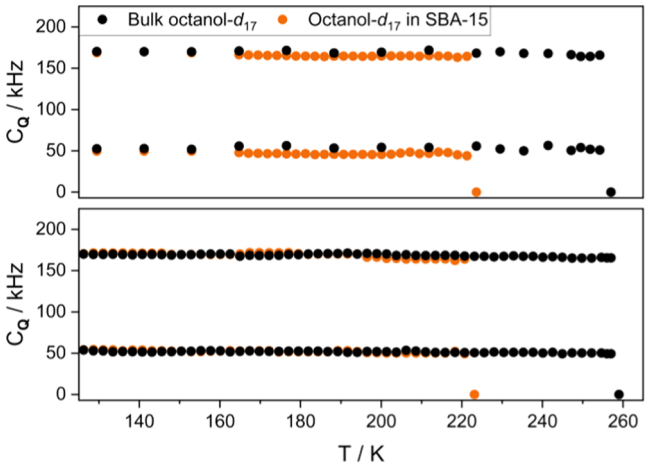

Figure 5. Values of C_Q extracted from the ^{2}H MAS spectra (top) and the static spectra (bottom) for bulk octanol-d_{17} and octanol-d_{17} in SBA-15.

that the motionally narrowed Pake pattern is caused by the CD_3-group moving around its C_3-axis in a 3-fold jump.[57] The determined values for C_Q are similar across both methods, confirming that the samples show an analogous behavior under MAS and static conditions. In addition, the octanol-d_{17} in SBA-15 does not show a considerably different quadrupolar coupling constant than the bulk octanol-d_{17}, suggesting that the vibrational dynamics in confinement are not significantly different than the dynamics in the bulk material. A detailed discussion of the influence of vibrational dynamics on the quadrupolar coupling constant is beyond the scope of this paper and can be found in the literature.[55,58] Interestingly, the quadrupolar coupling constants of the Pake patterns do not change considerably throughout the observed period, indicating that there are no changes in the dynamics of the corresponding molecules up to the melting point. This suggests that the molecules in the bulk octanol-d_{17}, as well as the octanol-d_{17} in SBA-15, are rather rigid, not allowing for an observable rotation of the entire molecule[9] or groups apart from the CD_3-group even at higher temperatures. Such dynamics would drastically alter the line shape, which cannot be observed here.[58] Considering the amphiphilic nature of the octanol-d_{17} molecule and the way it is packed when frozen in bulk[51] and when confined in mesoporous SBA-15,[10] the molecule is probably held in place by interactions of its OH-groups with each other and the OH-groups on the surface of the mesoporous silica. This results in the octanol-d_{17} being bound to the surface via hydrogen bonds with the aliphatic moiety oriented toward the pore center, preventing movement away from the surface and orienting their structure, similar to what was proposed recently by some of us.[10] This local order is transmitted to the inner parts of the pore, which also restricts the motional degrees of freedom of those octanol molecules, with the result that only the CD_3-group can perform fast rotations on the NMR time scale. Overall, it is likely that the majority of the confined octanol is in an aligned relative orientation that differs from bulk octanol based on the average pore size of about 6.5 nm (see Figure S1 in the Supporting Information) and the length of stretched n-octanol of about 1 nm based on the data supplied by crystallography.[51] Specifically, assuming the first two layers next to the pore surface are primarily structured in a bilayer form with the hydroxyl groups of the octanol layer next to surface aligned

https://doi.org/10.1021/acs.jpcc.1c05873
J. Phys. Chem. C 2021, 125, 25155−25164

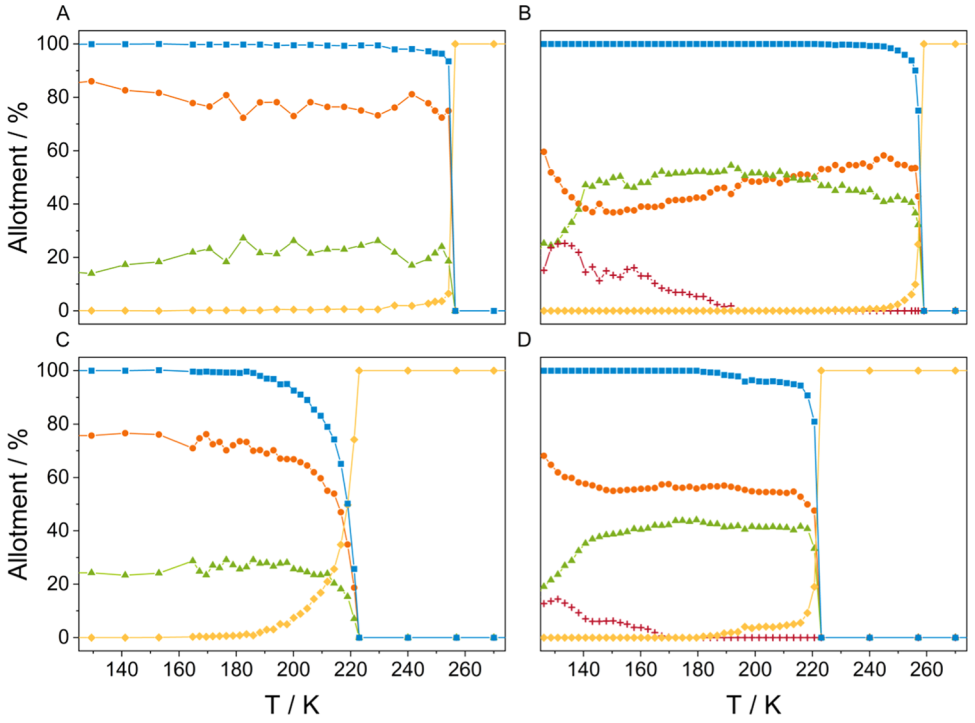

Figure 6. Relative intensities of the different components found in the samples. Orange circles: broad Pake pattern, green triangles: narrow Pake pattern, red crosses: non-Pake signal, yellow rhomb: isotropic signal, and blue squares: sum of the anisotropic signals. The non-Pake signal can only be found in the static spectra. Bulk octanol-d_{17} under MAS conditions (A), bulk octanol-d_{17} under static conditions (B), octanol-d_{17} in SBA-15 under MAS conditions (C), and octanol-d_{17} in SBA-15 under static conditions (D).

toward the surface and with opposite alignment for the second layer to maximize the hydrophobic interactions between the octanol tails, this would leave only a sphere of a diameter of 6.5 − 4 nm = 2.5 nm for the remaining octanol molecules to orient similarly as the bulk octanol does. A more detailed analysis of this model would require molecular dynamics simulations, which are beyond the scope of the present paper.

Fitting each component of the ^{2}H NMR spectra allows for a determination of the relative intensities of the respective components. Figure 6 shows the relative intensities of the solid and the liquid portions of the samples as well as all other observed spectral components (see Figure 6) as a function of the sample temperature T. The integrals of each signal can be used as a quantification of the number of deuterons, which are in the corresponding state of dynamics.

The data of bulk octanol-d_{17} (Figure 6A,B) both show an abrupt decline of the solid portion of the sample at the melting temperature, indicating a relatively quick transition between the solid and liquid phases. The spectra of the confined octanol-d_{17} (Figure 6C,D) both show an earlier onset of the melting process (about 30 K before the actual melting point) with a slow increase of the Lorentzian signal until a full melting of the sample can be observed.

The ratio of the broad and the narrow Pake patterns presented in Figure 6 can be compared to the theoretical ratios that result from the stoichiometry of the utilized octanol-d_{17}. Considering the narrow Pake pattern results from the methyl group of the aliphatic moiety of the molecule, it is expected to make up 17.6% of the observed signal, compared to 82.4% caused by the rest of the aliphatic deuterons. These ratios can only be observed at low temperatures in the bulk MAS spectra (Figure 6A, 130 K). All other spectra show a larger intensity of the signal caused by the methyl group and, in turn, a smaller signal caused by the methylene groups. These differences to the theoretical ratios are attributed to dynamics in the system. As mentioned previously, in the case of octanol-d_{17} under MAS (Figure 6A,C), the non-Pake signal cannot be observed. However, considering the presented ratios, the explanation of a signal corresponding to deuterons in the intermediate exchange regime being broadened and therefore not being observable on the MAS time scale is probable. This suspected broad signal would have its peak around the center of the spectrum, causing the observed increase of intensity (to about 25%) of the narrow Pake pattern.

A similar phenomenon is observed in the case of the static spectra. At low temperatures, they show smaller allotments than expected for the broad Pake pattern of 66% for the bulk and 74% for the confined octanol-d_{17}. However, they also display smaller ratio for the narrow Pake pattern with 13 and 12%, respectively. The rest of the signal is made up of the non-Pake component, which disappears gradually with increasing temperatures while the Lorentzian signal appears. Considering the non-Pake pattern is attributed to deuterons in the intermediate exchange regime and possibly less ordered octanol-d_{17} molecules, it is probable that these disordered molecules become mobile before the more ordered portion of molecules.[10,53] However, the intensity ratios are possibly distorted by parts of the signal not being refocused by the solid-echo pulse sequence, leading to potential loss of intensity.[55] Therefore, further investigations into the cause of the deviating intensity ratios in the static case are necessary to confirm the presented conclusion.

The differences in the melting behavior of the confined and bulk samples can be explained by the interaction of the octanol-d_{17} molecules with the surface of the mesoporous SBA-15 and the steric hindrances of the confinement. The

https://doi.org/10.1021/acs.jpcc.1c05873
J. Phys. Chem. C 2021, 125, 25155−25164

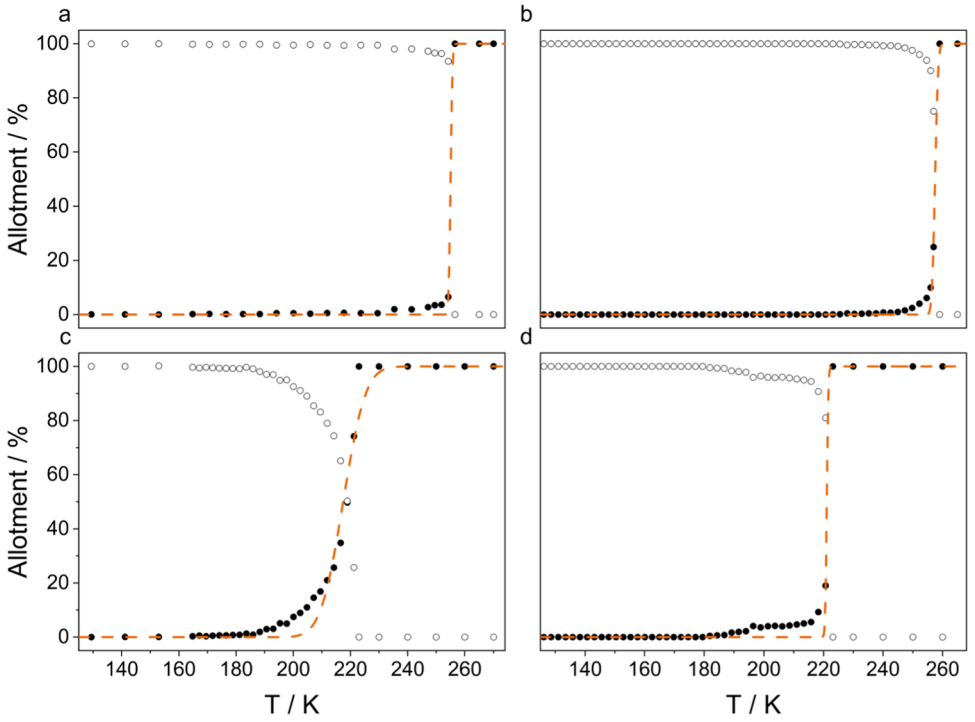

Figure 7. Relative intensities of the anisotropic (white circles) and Lorentzian parts caused by the isotropically moving molecules (solid circles) of the samples, including the calculated fits according to eq 3 (dashed line). Bulk octanol-d_{17} under MAS conditions (a), bulk octanol-d_{17} under static conditions (b), octanol-d_{17} in SBA-15 under MAS conditions (c), and octanol-d_{17} in SBA-15 under static conditions (d). Above the melting temperatures, additional points are extrapolated to stabilize the fitting procedure.

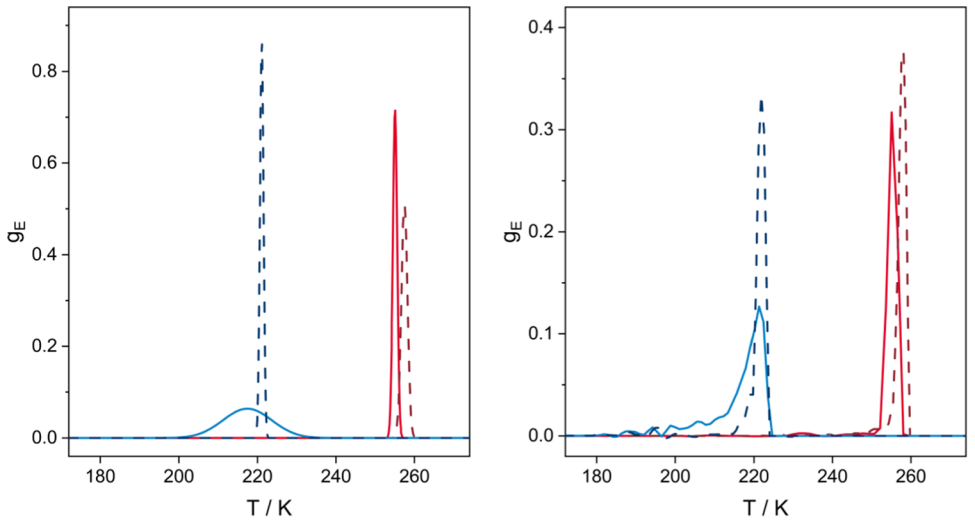

Figure 8. First derivatives of the fitting curves (left) and the experimental data (right) displayed in Figure 7 according to eq 4. Blue: octanol-d_{17} in SBA-15, red: bulk octanol-d_{17}, solid lines: MAS conditions, and dashed lines: static conditions.

confinement creates a distribution of locally different environments for the guest molecules, leading to a broad distribution of activation energies in the melting process. The fraction of molecules with lower activation energies has an earlier onset of their dynamics, therefore causing the observed changes of the intensity curves on the low-temperature side of the curves in Figure 6. We wish to note that similar dynamics occurring below the full melting point of the sample have also been observed for biphenyl.[59] However, considering the line shapes obtained from the DSC experiments, the formation of a continuous glass phase is unlikely,[60] making the formation of a glasslike pore solid the most viable explanation for the observed behavior. In these kinds of solids, the pores of the host material inhibit the formation of large, bulklike crystals, therefore lowering the equilibrium melting point of the confined material, $T_{m,c}$ in accordance with the Gibbs–Thomson equation (eq 2).[52] Equation 2 takes into account the bulk melting temperature, $T_{m,b}$, as well as the surface energy of the solid–liquid interface, σ_{sl}, the enthalpy of melting, H_m, the density of the corresponding solid, ρ, and the radius of the crystal, r, to calculate the melting point suppression ΔT_m.

https://doi.org/10.1021/acs.jpcc.1c05873
J. Phys. Chem. C 2021, 125, 25155−25164

$$\Delta T_m = T_{m,b} - T_{m,c} = T_{m,b}\frac{2\sigma_{sl}}{H_m \rho\, r} \quad (2)$$

In the case of a broad distribution of activation energies, the distribution function can be determined by fitting the relative intensities of the isotropic component according to Rössler et al.,[40] assuming in the simplest case a Gaussian distribution of activation energies g_E and employing the fraction of isotropically moving molecules c_{iso}, the melting point T_0 as the center of gravity, and ΔT as the width of the distribution (eq 3). This approach was previously used to accurately describe the dynamics of, e.g., confined benzene-d_6,[9,40] biphenyl,[59] and hexamethylbenzene-d_{18}[40] molecules.

$$c_{iso} = \int_0^T \frac{1}{\sqrt{2\pi\Delta T^2}}\exp\left(-\frac{(T-T_0)^2}{2\Delta T^2}\right)dT = \frac{1}{2}\mathrm{erf}\left(\frac{1}{\sqrt{2}\,\Delta T}(T-T_0)\right) + \frac{1}{2}\mathrm{erf}\left(\frac{1}{\sqrt{2}\,\Delta T}T_0\right) \quad (3)$$

By calculating the derivative of eq 3, a distribution of activation energies in temperature units (eq 4) is obtained.

$$g_E = \frac{d}{dT}c_{iso} = \frac{1}{\sqrt{2\pi}\,\Delta T}\exp\left(-\frac{(T-T_0)^2}{2\Delta T^2}\right) \quad (4)$$

The corresponding graphical representation of this approach is shown in Figures 7 and 8. While for glasslike systems with a clear separation between rotational and translational degrees of freedom, a direct conversion of the temperature distributions to activation energy distributions is feasible via the two-phase model developed by Rössler et al.,[40] in the present case, these degrees of freedom are coupled. Thus, the applicability of the model by Rössler et al.[40] in the present case is limited, and a detailed interpretation of the distribution curves would necessitate molecular dynamics simulations, which are beyond the scope of this paper. Therefore, Figure 8 displays the corresponding distribution in temperature units. Additionally, the derivative of the experimental data is calculated and plotted to illustrate potential differences between the idealized fit and the measured intensities.

Generally, the data presented in Figures 7 and 8 follow the expectations described earlier. The distributions of activation energies for the bulk octanol-d_{17} (obtained from Figures 7a,b and 8 left, red lines) are narrow, indicating the melting of a crystalline solid.[40] The distribution of activation energies for the confined octanol-d_{17} obtained under MAS conditions is broad (Figure 8 left, blue solid line), denoting a melting process involving species in different environments and possibly a distribution of rigidly and less rigidly ordered molecules.[16,52] On the low-temperature flanks of the obtained melting curves for the confined octanol-d_{17} (Figure 7c,d), there are clear deviations between the experimental and calculated curves, revealing a non-Gaussian distribution of activation energies and again illustrating that the used model may only be used as an approximation.

Additionally, this non-Gaussian distribution is illustrated by the numerical derivative of the experimental data (Figure 8 right), especially for the confined octanol-d_{17} under MAS conditions. For this sample, a shoulder on the low-temperature flank of the main curve is visible, indicating lower melting points for the molecules involved in the premelting process compared to the full melting.

CONCLUSIONS

In this work, DSC and ^{2}H solid-state NMR in combination with numerical modeling of the obtained data were applied to investigate the behavior of octanol-d_{17} in bulk as well as in confinement in mesoporous SBA-15 starting at 125 K, up to the melting point of the respective sample. The composition of the samples and quadrupolar coupling constants at any given temperature were determined for the MAS and the static case and used to elucidate the dynamics of the system. It could be demonstrated that both the bulk as well as the confined octanol-d_{17} are held in place by the interplay of hydrogen bonds and dispersion forces, resulting in the rotation of the CD_3-group around its C_3-axis as the only active motional degree of freedom. Differences occur in the region shortly before the melting point. Bulk octanol-d_{17} shows a behavior typical for crystalline solids, melting at once at its melting temperature. Confined octanol-d_{17} shows a slow melting process with an onset of 30 K before its melting point due to the interactions of the molecule with the rough surface of the mesoporous material, leading to a broad, non-Gaussian distribution of activation energies for the melting process. Additionally, the melting temperature of the confined octanol-d_{17} is about 38 K lower, suggesting a smaller crystallite size than in bulk in accordance with the Gibbs−Thomson equation and therefore the formation of a pore solid[52] with a potentially amorphous portion. The presented findings serve as an example of the dynamics of linear small amphiphilic organic molecules and may be applicable to similar systems like amines or carboxylic acids.

ASSOCIATED CONTENT

Supporting Information

The Supporting Information is available free of charge at https://pubs.acs.org/doi/10.1021/acs.jpcc.1c05873.

Information on utilized chemicals; nitrogen adsorption data; examples of ^{2}H MAS NMR spectra with non-absorbed octanol-d_{17}; and comparison of a symmetrized and a nonsymmetrized static ^{2}H NMR spectrum of bulk octanol-d_{17} (PDF)

AUTHOR INFORMATION

Corresponding Author

Gerd Buntkowsky − *Eduard-Zintl-Institut für Anorganische und Physikalische Chemie, Technische Universität Darmstadt, D-64287 Darmstadt, Germany;* orcid.org/0000-0003-1304-9762; Phone: +49 6151 16 21116; Email: gerd.buntkowsky@chemie.tu-darmstadt.de

Authors

Sonja C. Döller − *Eduard-Zintl-Institut für Anorganische und Physikalische Chemie, Technische Universität Darmstadt, D-64287 Darmstadt, Germany*

Martin Brodrecht − *Eduard-Zintl-Institut für Anorganische und Physikalische Chemie, Technische Universität Darmstadt, D-64287 Darmstadt, Germany*

Nadia B. Haro Mares − *Eduard-Zintl-Institut für Anorganische und Physikalische Chemie, Technische Universität Darmstadt, D-64287 Darmstadt, Germany*

Hergen Breitzke − *Eduard-Zintl-Institut für Anorganische und Physikalische Chemie, Technische Universität Darmstadt, D-64287 Darmstadt, Germany*

https://doi.org/10.1021/acs.jpcc.1c05873
J. Phys. Chem. C 2021, 125, 25155−25164

Torsten Gutmann − *Eduard-Zintl-Institut für Anorganische und Physikalische Chemie, Technische Universität Darmstadt, D-64287 Darmstadt, Germany;* orcid.org/0000-0001-6214-2272

Markus Hoffmann − *Department of Chemistry and Biochemistry, State University of New York College at Brockport, Brockport, New York 14420, United States;* orcid.org/0000-0002-5469-8665

Complete contact information is available at: https://pubs.acs.org/10.1021/acs.jpcc.1c05873

Notes

The authors declare no competing financial interest.

■ ACKNOWLEDGMENTS

Financial support by the Deutsche Forschungsgemeinschaft under Contract Bu-911-24-2 and by the National Science Foundation under Grant No. 1953428 are gratefully acknowledged.

■ REFERENCES

(1) Andanson, J.-M.; Baiker, A. Exploring Catalytic Solid/Liquid Interfaces by in Situ Attenuated Total Reflection Infrared Spectroscopy. *Chem. Soc. Rev.* **2010**, *39*, 4571−4584.

(2) François, I.; Sandra, K.; Sandra, P. Comprehensive Liquid Chromatography: Fundamental Aspects and Practical Considerations—a Review. *Anal. Chim. Acta* **2009**, *641*, 14−31.

(3) Zhou, P.; Yao, L.; Chen, K.; Su, B. Silica Nanochannel Membranes for Electrochemical Analysis and Molecular Sieving: A Comprehensive Review. *Crit. Rev. Anal. Chem.* **2020**, *50*, 424−444.

(4) Murillo-Cremaes, N.; López-Periago, A. M.; Saurina, J.; Roig, A.; Domingo, C. Nanostructured Silica-based Drug Delivery Vehicles for Hydrophobic and Moisture Sensitive Drugs. *J. Supercrit. Fluids* **2013**, *73*, 34−42.

(5) Ahmaruzzaman, M. Industrial Wastes as Low-Cost Potential Adsorbents for the Treatment of Wastewater Laden with Heavy Metals. *Adv. Colloid Interface Sci.* **2011**, *166*, 36−59.

(6) Sun, B.; Zhou, G.; Zhang, H. Synthesis, Functionalization, and Applications of Morphology-controllable Silica-based Nanostructures: A Review. *Prog. Solid State Chem.* **2016**, *44*, 1−19.

(7) Zhao, D.; Feng, J.; Huo, Q.; Melosh, N.; Fredrickson, G. H.; Chmelka, B. F.; Stucky, G. D. Triblock Copolymer Syntheses of Mesoporous Silica with Periodic 50 to 300 Angstrom Pores. *Science* **1998**, *279*, 548−552.

(8) Beck, J. S.; Vartuli, J. C.; Roth, W. J.; Leonowicz, M. E.; Kresge, C. T.; Schmitt, K. D.; Chu, C. T. W.; Olson, D. H.; Sheppard, E. W.; McCullen, S. B.; et al. A New Family of Mesoporous Molecular Sieves Prepared with Liquid Crystal Templates. *J. Am. Chem. Soc.* **1992**, *114*, 10834−10843.

(9) Gedat, E.; Schreiber, A.; Albrecht, J.; Emmler, T.; Shenderovich, I.; Findenegg, G. H.; Limbach, H.-H.; Buntkowsky, G. 2H-Solid-State NMR Study of Benzene-d6 Confined in Mesoporous Silica SBA-15. *J. Phys. Chem. B* **2002**, *106*, 1977−1984.

(10) Kumari, B.; Brodrecht, M.; Breitzke, H.; Werner, M.; Grünberg, B.; Limbach, H.-H.; Forg, S.; Sanjon, E. P.; Drossel, B.; Gutmann, T.; et al. Mixtures of Alcohols and Water confined in Mesoporous Silica: A Combined Solid-State NMR and Molecular Dynamics Simulation Study. *J. Phys. Chem. C* **2018**, *122*, 19540−19550.

(11) Buntkowsky, G.; Breitzke, H.; Adamczyk, A.; Roelofs, F.; Emmler, T.; Gedat, E.; Grünberg, B.; Xu, Y.; Limbach, H.-H.; Shenderovich, I.; et al. Structural and Dynamical Properties of Guest Molecules Confined in Mesoporous Silica Materials Revealed by NMR. *Phys. Chem. Chem. Phys.* **2007**, *9*, 4843−4853.

(12) Hassan, J. Analysis of 2H NMR Spectra of Water Molecules on the Surface of Nano-silica Material MCM-41: Deconvolution of the Signal Into a Lorentzian and a Powder Pattern Line Shapes. *Phys. B* **2012**, *407*, 179−183.

(13) Ben Shir, I.; Kababya, S.; Schmidt, A. Binding Specificity of Amino Acids to Amorphous Silica Surfaces: Solid-State NMR of Glycine on SBA-15. *J. Phys. Chem. C* **2012**, *116*, 9691−9702.

(14) Amitay-Rosen, T.; Vega, S. A Deuterium MAS NMR Study of the Local Mobility of Dissolved Methionine and di-Alanine at the Inner Surface of SBA-15. *Phys. Chem. Chem. Phys.* **2010**, *12*, 6763−6773.

(15) Amitay-Rosen, T.; Kababya, S.; Vega, S. A Dynamic Magic Angle Spinning NMR Study of the Local Mobility of Alanine in an Aqueous Environment at the Inner Surface of Mesoporous Materials. *J. Phys. Chem. B* **2009**, *113*, 6267−6282.

(16) Dosseh, G.; Xia, Y.; Alba-Simionesco, C. Cyclohexane and Benzene Confined in MCM-41 and SBA-15: Confinement Effects on Freezing and Melting. *J. Phys. Chem. B* **2003**, *107*, 6445−6453.

(17) Alba-Simionesco, C.; Coasne, B.; Dosseh, G.; Dudziak, G.; Gubbins, K. E.; Radhakrishnan, R.; Sliwinska-Bartkowiak, M. Effects of Confinement on Freezing and Melting. *J. Phys.: Condens. Matter* **2006**, *18*, R15−R68.

(18) Palombo, F.; Sassi, P.; Paolantoni, M.; Morresi, A.; Cataliotti, R. S. Comparison of Hydrogen Bonding in 1-Octanol and 2-Octanol as Probed by Spectroscopic Techniques. *J. Phys. Chem. B* **2006**, *110*, 18017−18025.

(19) Hu, K.; Zhou, Y.; Shen, J.; Ji, Z.; Cheng, G. Micro-heterogeneous Structure of 1-Octanol in Neat and Water-Saturated State. *J. Phys. Chem. B* **2007**, *111*, 10160−10165.

(20) Franks, N. P.; Abraham, M. H.; Lieb, W. R. Molecular Organization of Liquid n-Octanol: An X-ray Diffraction Analysis. *J. Pharm. Sci.* **1993**, *82*, 466−470.

(21) Huyskens, P.; Ruelle, P. Dynamic Equilibrium Time Fractions or Fractional Lifetimes? The Final Chapter. *J. Mol. Liq.* **2000**, *88*, 87−108.

(22) de Oliveira, C. A. F.; Guimarães, C. R. W.; Bicca de Alencastro, R. Molecular Dynamics Study on Liquid 1-Octanol. Part 2. Water-Saturated 1-Octanol Solution. *Int. J. Quantum Chem.* **2002**, *90*, 786−791.

(23) Chen, B.; Siepmann, J. I. Microscopic Structure and Solvation in Dry and Wet Octanol. *J. Phys. Chem. B* **2006**, *110*, 3555−3563.

(24) Marcus, Y. Structural Aspects of Water in 1-Octanol. *J. Solution Chem.* **1990**, *19*, 507−517.

(25) Zana, R.; Talmon, Y. Dependence of Aggregate Morphology on Structure of Dimeric Surfactants. *Nature* **1993**, *362*, 228−230.

(26) Kancharla, S.; Canales, E.; Alexandridis, P. Perfluorooctanoate in Aqueous Urea Solutions: Micelle Formation, Structure, and Microenvironment. *Int. J. Mol. Sci.* **2019**, *20*, 5761−5778.

(27) Manne, S.; Gaub, H. E. Molecular Organization of Surfactants at Solid-Liquid Interfaces. *Science* **1995**, *270*, 1480−1482.

(28) Lamont, R. E.; Ducker, W. A. Surface-Induced Transformations for Surfactant Aggregates. *J. Am. Chem. Soc.* **1998**, *120*, 7602−7607.

(29) Zaera, F. Probing Liquid/Solid Interfaces at the Molecular Level. *Chem. Rev.* **2012**, *112*, 2920−2986.

(30) Hind, A. R.; Bhargava, S. K.; McKinnon, A. At the Solid/Liquid Interface: Ftir/Atr — the Tool of Choice. *Adv. Colloid Interface Sci.* **2001**, *93*, 91−114.

(31) Zou, S.; Williams, C. T.; Chen, E. K.-Y.; Weaver, M. J. Probing Molecular Vibrations at Catalytically Significant Interfaces: A New Ubiquity of Surface-Enhanced Raman Scattering. *J. Am. Chem. Soc.* **1998**, *120*, 3811−3812.

(32) Raposo, M.; Pontes, R. S.; Mattoso, L. H. C.; Oliveira, O. N. Kinetics of Adsorption of Poly(o-methoxyaniline) Self-Assembled Films. *Macromolecules* **1997**, *30*, 6095−6101.

(33) Serrano, A. G.; Cabré, E. J.; Oviedo, J. M.; Cruz, A.; González, B.; Palacios, A.; Estrada, P.; Pérez-Gil, J. Production in Escherichia Coli of a Recombinant C-terminal Truncated Precursor of Surfactant Protein B (Rprosp-b Delta C). Structure and Interaction With Lipid Interfaces. *Biochim. Biophys. Acta, Biomembr.* **2006**, 1621−1632.

(34) Fenter, P.; Sturchio, N. C. Mineral-water Interfacial Structures Revealed by Synchrotron X-ray Scattering. *Prog. Surf. Sci.* **2004**, *77*, 171−258.
(35) Alba-Simionesco, C.; Dosseh, G.; Dumont, E.; Frick, B.; Geil, B.; Morineau, D.; Teboul, V.; Xia, Y. Confinement of Molecular Liquids: Consequences on Thermodynamic, Static and Dynamical Properties of Benzene and Toluene. *Eur. Phys. J. E* **2003**, *12*, 19−28.
(36) Werner, M.; Rothermel, N.; Breitzke, H.; Gutmann, T.; Buntkowsky, G. Recent Advances in Solid State NMR of Small Molecules in Confinement. *Isr. J. Chem.* **2014**, *54*, 60−73.
(37) de Oliveira, C. A. F.; Guimares, C. R. W.; de Alencastro, R. B. Molecular Dynamics Study on Liquid 1-Octanol. *Int. J. Quantum Chem.* **2000**, *80*, 999−1006.
(38) Sassi, P.; Paolantoni, M.; Cataliotti, R. S.; Palombo, F.; Morresi, A. Water/Alcohol Mixtures: A Spectroscopic Study of the Water-Saturated 1-Octanol Solution. *J. Phys. Chem. B* **2004**, *108*, 19557−19565.
(39) Kissinger, H. E. Variation of Peak Temperature With Heating Rate In Differential Thermal Analysis. *J. Res. Natl. Bur. Stand.* **1956**, *57*, 217−221.
(40) Rössler, E.; Taupitz, M.; Börner, K.; Schulz, M.; Vieth, H.-M. A Simple Method Analyzing 2H Nuclear Magnetic Resonance Line Shapes to Determine the Activation Energy Distribution of Mobile Guest Molecules in Disordered Systems. *J. Chem. Phys.* **1990**, *92*, 5847−5855.
(41) Buntkowsky, G.; Vogel, M. Small Molecules, Non-Covalent Interactions, and Confinement. *Molecules* **2020**, *25*, 3311−3343.
(42) Brodrecht, M.; Breitzke, H.; Gutmann, T.; Buntkowsky, G. Biofunctionalization of Nano Channels by Direct In-Pore Solid-Phase Peptide Synthesis. *Chem. - Eur. J.* **2018**, *24*, 17814−17822.
(43) Wang, X.; Lin, K. S. K.; Chan, J. C. C.; Cheng, S. Direct Synthesis and Catalytic Applications of Ordered Large Pore Aminopropyl-Functionalized SBA-15 Mesoporous Materials. *J. Phys. Chem. B* **2005**, *109*, 1763−1769.
(44) Brunauer, S.; Emmett, P. H.; Teller, E. Adsorption of Gases in Multimolecular Layers. *J. Am. Chem. Soc.* **1938**, *60*, 309−319.
(45) Klyachko-Gurvich, A. L. An Improved Method of Determining Surface Area by the Adsorption of Air. *Bull. Acad. Sci. USSR, Div. Chem. Sci.* **1961**, *10*, 1756−1758.
(46) Barrett, E. P.; Joyner, L. G.; Halenda, P. P. The Determination of Pore Volume and Area Distributions in Porous Substances. I. Computations from Nitrogen Isotherms. *J. Am. Chem. Soc.* **1951**, *73*, 373−380.
(47) Bielecki, A.; Burum, D. P. Temperature Dependence of 207 Pb MAS Spectra of Solid Lead Nitrate. An Accurate, Sensitive Thermometer for Variable-Temperature MAS. *J. Magn. Reson., Ser. A* **1995**, *116*, 215−220.
(48) Massiot, D.; Fayon, F.; Capron, M.; King, I.; Le Calvé, S.; Alonso, B.; Durand, J.-O.; Bujoli, B.; Gan, Z.; Hoatson, G. Modelling One- and Two-dimensional Solid-state NMR Spectra. *Magn. Reson. Chem.* **2002**, *40*, 70−76.
(49) Vyazovkin, S. Is the Kissinger Equation Applicable to the Processes that Occur on Cooling? *Macromol. Rapid Commun.* **2002**, *23*, 771−775.
(50) Xia, Y.; Dosseh, G.; Morineau, D.; Alba-Simionesco, C. Phase Diagram and Glass Transition of Confined Benzene. *J. Phys. Chem. B* **2006**, *110*, 19735−19744.
(51) Shallard-Brown, H. A.; Watkin, D. J.; Cowley, A. R. n-Octanol. *Acta Crystallogr., Sect. E: Struct. Rep. Online* **2005**, *61*, o213−o214.
(52) Jackson, C. L.; McKenna, G. B. The Melting Behavior of Organic Materials Confined in Porous Solids. *J. Chem. Phys.* **1990**, *93*, 9002−9011.
(53) Wallacher, D.; Knorr, K. Melting and Freezing of Ar in Nanopores. *Phys. Rev. B* **2001**, *63*, No. 104202.
(54) Beshah, K.; Olejniczak, E. T.; Griffin, R. G. Deuterium NMR Study of Methyl Group Dynamics in L-alanine. *J. Chem. Phys.* **1987**, *86*, 4730−4736.
(55) Spiess, H.; Sillescu, H. Solid Echoes in the Slow-Motion Region. *J. Magn. Reson.* **1981**, *42*, 381−389.
(56) Millett, F. S.; Dailey, B. P. NMR Determination of Some Deuterium Quadrupole Coupling Constants in Nematic Solutions. *J. Chem. Phys.* **1972**, *56*, 3249−3256.
(57) Polson, J. M.; Fyfe, J. D. D.; Jeffrey, K. R. The Reorientation of t-Butyl Groups in Butylated Hydroxytoluene: A Deuterium Nuclear Magnetic Resonance Spectral and Relaxation Time Study. *J. Chem. Phys.* **1991**, *94*, 3381−3388.
(58) Schmidt-Rohr, K.; Spiess, H. W. *Multidimensional Solid-State NMR and Polymers*; Academic Press: London, 2005.
(59) de Sousa Amadeu, N.; Grünberg, B.; Frydel, J.; Werner, M.; Limbach, H.-H.; Breitzke, H.; Buntkowsky, G. Melting of Low Molecular Weight Compounds in Confinement Observed by 2H-Solid State NMR: Biphenyl, a Case Study. *Z. Phys. Chem.* **2012**, *226*, 1169−1186.
(60) Gill, P.; Moghadam, T. T.; Ranjbar, B. Differential Scanning Calorimetry Techniques: Applications in Biology and Nanoscience. *J. Biomol. Tech.* **2010**, *21*, 167−193.

https://doi.org/10.1021/acs.jpcc.1c05873
J. Phys. Chem. C 2021, 125, 25155−25164